Chapter 5

LONGITUDINAL MICROWAVE INSTABILITY FOR PROTONS

The equation of motion for the longitudinal coordinate τ of a particle can be obtained from Eqs. (3.10) and (3.11):

$$\frac{d^2\tau}{ds^2} + \frac{\omega_s^2}{v^2}\tau = -\frac{\eta}{v\beta^2 E_0}\langle F_0^{\parallel}(\tau)\rangle \ . \tag{5.1}$$

For a reactive wake function $W_0'(z) = L\delta'(z/v)$, it reduces to

$$\frac{d^2\tau}{ds^2} + \frac{\omega_s^2}{v^2}\tau = -\frac{e^2\eta L}{v\beta^2 C E_0}\rho'(\tau) \ . \tag{5.2}$$

For a rather long and uniform bunch, the slope of the linear distribution is mostly zero. Now suppose a small bump appears in the linear density with distribution $\rho(\tau)$. The front of the bump has $\rho'(\tau) < 0$ and the rear $\rho'(\tau) > 0$. For an inductive wake ($L > 0$) above transition ($\eta > 0$) or a capacitive wake below transition, particles at the front of the bump accelerate and gain energy, while those at the rear will decelerate and lose energy. In the next accelerator turn, the front particles will arrive earlier while the rear particles later, resulting in the smoothing out of the bump. This is illustrated in the left drawing in Fig. 5.1. However, for an inductive wake below transition or a capacitive wake above transition, particles at the front of the bump decelerate and those at the rear accelerate, thus enhancing the bump. In other word, the situation is unstable against small nonuniformity in the linear distribution. In order for the bump to grow, the growth rate must be faster than phase-drifting rate coming from the momentum spread of the

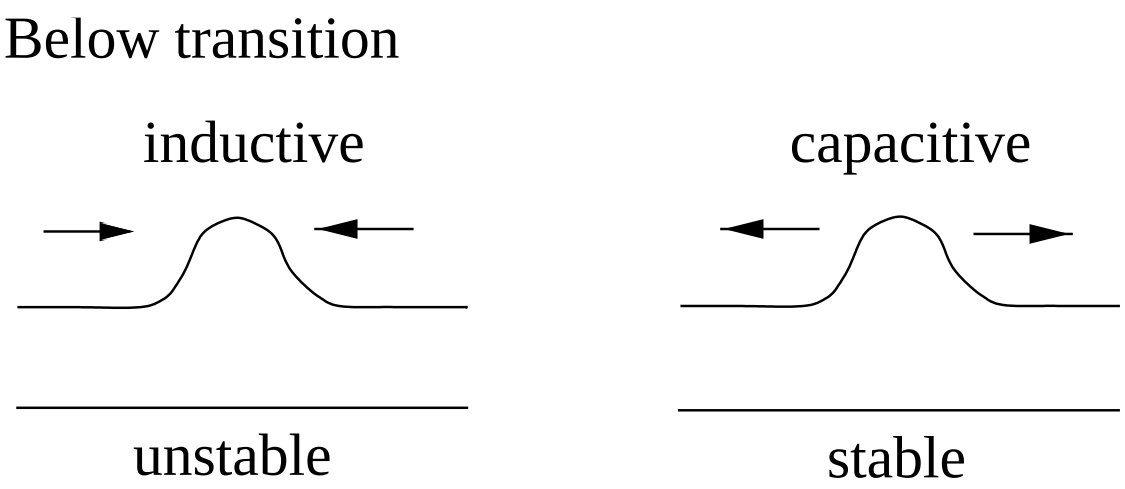

Figure 5.1: Below transition, a bump will be smoothed out under a capacitive force (right) and the beam will be stable against bump formation. However under an inductive force, the bump will continue to grow (left) and the beam will be unstable against small perturbations. Above transition, the opposite will be true.

beam. This damping process is called *Landau damping* [1]. For a bunch, the growth must be faster than synchrotron frequency otherwise the bump will be smeared out. Also since the size of the bump must be less than the length of the bunch, the impedance driving the instability must have a wavelength less than the length of the bunch. This growth at high frequencies is called *microwave instability*. This discussion is very similar to that in Sec. 4.2. There, the concern is about the enhancement or partial cancellation of the rf focusing force at rf frequency; therefore an inductive force below transition or a capacitive force above transition is preferred. Here, the concern is the evolution of a small bump at high frequencies. In order that a small bump will not grow, the opposite conclusion is obtained. In other words, a capacitive force below transition or an inductive force above transition is preferred.

Because of the random quantum excitation in the electron bunch, there is a finite probability of having electrons jumping outside the bucket and getting lost. To increase the *quantum lifetime* of an electron bunch, the rf bucket has to be large. Also Touschek scattering will convert transverse momentum spread of electrons into longitudinal. In order that those electrons will not be lost, the rf bucket has to be large. For this reason, the bucket in an electron machine is in general very much larger than the size of the electron bunch, usually the height of the bucket is more than 10 times the rms energy spread of the bunch. To achieve this, the rf voltage $V_{\rm rf}$ for an electron ring will be relatively

much larger than that in a proton ring of the same energy. Another reason of a high $V_{\rm rf}$ in an electron machine is to compensate for the energy loss due to synchrotron radiation. For example, in the high-energy ring of PEP II storing 9 GeV electrons, $V_{\rm rf} = 18.5$ MV is required. On the other hand, $V_{\rm rf}$ for the Fermilab Tevatron storing 1 TeV protons is only 2.16 MV. As a result, the synchrotron tunes for electron rings, $\nu_s \sim 0.01$, are usually an order of magnitude larger than those for proton rings, $\nu_s \sim 0.001$. For this reason, in the consideration of collective instabilities, the synchrotron period of the protons is sometimes much longer than the instability growth times. Also the wavelength of the perturbation or instability driving force is often of the same size as the radius or diameter of the vacuum chamber, which is usually much shorter than the length of a proton bunch. As a result, the proton bunches can be viewed locally as coasting beams in many instability considerations. Thus, each individual revolution harmonic can be considered as an independent mode. On the other hand, the electron bunch is mostly short, of the same size or even shorter than the diameter of the vacuum chamber. In other words, the electron bunch length can be of the same order or even shorter than the wavelength of the instability driving force. Therefore, for electron bunches, their bunch structure must be considered when studying their instabilities. Individual revolution harmonics are no longer independent and we need to study bunch modes instead.

5.1 DISPERSION RELATION

Let us first study the dispersion relation governing microwave instability of a proton beam [2]. Consider a coasting beam, i.e., $\omega_s = 0$, with the unperturbed phase-space distribution

$$\psi_0(\Delta E) = \frac{N}{T_0} f_0(\Delta E) \ , \tag{5.3}$$

where $f_0(\Delta E)$ is normalized to unity when integrated over ΔE, and $T_0 = 2\pi/\omega_0$ is the revolution period of an on-momentum particle. Since the linear distribution is uniform, it does not depends on the location s along the circumference of ring or the time t of evolution. This stationary distribution is perturbed by an infinitesimal longitudinal density wave ψ_1 which is position dependent and evolves in time. At time t, we postulate the ansatz

$$\psi_1(s, t, \Delta E) = \hat{\psi}_1(\Delta E) e^{ins/R - i\Omega t} \ , \tag{5.4}$$

where $R = C/(2\pi)$ is mean radius of the closed orbit of an on-momentum particle, and $\Omega/(2\pi)$ the collective frequency of oscillation to be determined. Here, n denotes the

revolution harmonic and $n = 0$ must be excluded, otherwise charge conservation will be violated. By ansatz, we mean a postulation of the solution which must be verified to be consistent later. In fact, Eq. (5.4) is just one term of a Fourier series expansion. For that reason, our postulation is the independence of each revolution harmonic or the revolution harmonic is a good eigen-number. When integrated over ΔE, we get the perturbation line density at some time t,

$$\rho_1(s,t) = \hat{\rho}_1 e^{ins/R - i\Omega t} \ . \tag{5.5}$$

A particle at location s and time t sees a wake force due to all beam particles that pass the same location at an earlier time $t - z/v$. This force, averaged over the ring circumference, can be expressed as

$$\langle F_0^{\parallel}(s,t)\rangle = -\frac{e^2}{C}\int_0^{\infty}\frac{dz}{v}\,\rho_1(s,t-z/v)W_0'(z) = -\frac{e^2}{C}\,\rho_1(s,t)Z_0^{\parallel}(\Omega) \ , \tag{5.6}$$

where $Z_0^{\parallel}(\Omega)$ is the longitudinal impedance of the vacuum chamber evaluated at the collective frequency. Note that here we are using t as the independent variable, because there is no complication arising from synchrotron oscillation. Actually, this is a snap-shot description. If not there will not be periodicity of s in the ring circumference. There is a similar force acting from the particle from the wake of the unperturbed beam distribution [$\rho_1 \to \rho_0$ in Eq. (5.6)]. But that force has no time dependency and is of no interest to us here. In fact, this force will give a modified steady-state Hamiltonian and will contribute to the a modification of the unperturbed particle distribution, which we call potential-well distortion.

The particle energy will be perturbed according to the equation of motion Eq. (3.5)

$$\frac{d\Delta E}{dt} = -\frac{e^2}{T_0}Z_0^{\parallel}(\Omega)\hat{\rho}_1 e^{ins/R - i\Omega t} \ , \tag{5.7}$$

where $T_0 = 2\pi/\omega_0$ is the revolution period of the on-momentum particles.

Now let us pull out the Vlasov equation in its first order,

$$\frac{\partial\psi_1}{\partial t} + \frac{\partial\psi_1}{\partial s}\frac{ds}{dt} + \frac{\partial\psi_0}{\partial\Delta E}\frac{d\Delta E}{dt} = 0 \ . \tag{5.8}$$

Substitution leads to

$$-i(\Omega - n\omega)\psi_1 = \frac{e^2 Z_0^{\parallel}(\Omega)}{T_0}\frac{d\psi_0}{d\Delta E}\,\hat{\rho}_1 e^{ins/R - i\Omega t} \ , \tag{5.9}$$

where ω is the angular revolution frequency of a particle and is ΔE dependent. Next we have

$$\psi_1 = \frac{ie^2 Z_0^{\parallel}(\Omega)}{T_0} \frac{d\psi_0/d\Delta E}{\Omega - n\omega} \hat{\rho}_1 e^{ins/R - i\Omega t} \ . \tag{5.10}$$

Integrate both sides over ΔE. From Eq. (5.5), the left side just cancels $\hat{\rho}_1$ and the exponential on the right side, and we have

$$1 = \frac{ie^2 N Z_0^{\parallel}}{T_0^2} \int \frac{f_0'(\Delta E)}{\Omega - n\omega} \, d\Delta E \ , \tag{5.11}$$

where this distribution f_0 in Eq. (5.3) that normalized to unity has been used. An integration by part leads to the dispersion relation

$$1 = \frac{ieI_0 \eta n Z_0^{\parallel}(\Omega)\omega_0^2}{2\pi\beta^2 E_0} \int \frac{f_0(\Delta E)}{(\Omega - n\omega)^2} \, d\Delta E \ , \tag{5.12}$$

where the relation

$$\frac{d\omega}{d\Delta E} = -\frac{\eta\omega_0}{\beta^2 E_0} \tag{5.13}$$

has been used. The negative sign on the right side of Eq. (5.13) comes about because the revolution frequency decreases as energy increases above transition. An immediate conclusion of Eq. (5.12) is that our ansatz for ψ_1 in Eq. (5.4) is correct and all revolution harmonics are decoupled. Equation (5.12) is called a dispersion relation because it provides the relation of the collective frequency Ω to the wave number n/R. This collective frequency is to be solved from the dispersion relation for each revolution harmonic. If Ω has an imaginary part that is positive, the solution reveals a growth and there is a collective instability.

If there is no energy spread, the collective frequency can be solved easily. Above transition where $\eta > 0$,

$$\Omega = n\omega_0 + \sqrt{\frac{eI_0\eta n}{2\pi\beta^2 E_0}} \sqrt{i\,\mathcal{R}e\, Z_0^{\parallel}(\Omega) - \mathcal{I}m\, Z_0^{\parallel}(\Omega)}\, \omega_0 \ , \tag{5.14}$$

of which the positive imaginary part is the growth rate. We see that above transition there is no growth only when $Z_0^{\parallel}$ is purely inductive, as postulated at the beginning of the discussion. For a low-energy machine, the space-charge impedance per harmonic is frequency independent and rolls off only at very high frequencies. Therefore above transition, the growth rate is directly proportional to n or frequency. This is the source of negative-mass instability for a proton machine just above transition.

Now let us consider a realistic beam that has an energy spread. Since ω is a function of the energy offset ΔE, define a revolution frequency distribution $g_0(\omega)$ for the unperturbed beam such that

$$g_0(\omega)d\omega = f_0(\Delta E)d\Delta E \ . \tag{5.15}$$

Substituting into Eq. (5.12) and integrating by part, we obtain

$$1 = -\frac{ieI_0\eta Z_0^{\parallel}(\Omega)\omega_0^2}{2\pi\beta^2 E_0}\int \frac{g_0'(\omega)}{\Omega - n\omega}\,d\omega \ . \tag{5.16}$$

Given the frequency distribution $g_0(\omega)$ of the unperturbed beam and the impedance $Z_0^{\parallel}$ of the ring at roughly $n\omega_0$, the collective frequency Ω can be solved from the dispersion equation. For a given revolution harmonic n, there can be many solutions for Ω. However, we are only interested in those that have positive imaginary parts. This is because if there is one such unstable solution, the system will be unstable independent of how many stable solutions there are. However, there is a subtlety in dealing with solution on the edge of stability, that is, when Ω is real. The dispersion relation will blow up when $n\omega = \Omega$ during the integration. This subtlety can be resolved if the problem is formulated as an initial value problem, which we will discuss in Chapter 14 on Landau damping. It will be shown that the proper way to go around the subtlety is to make the replacement

$$\Omega \longrightarrow \Omega + i\epsilon \ , \tag{5.17}$$

where ϵ is an infinitesimal positive real number. In other words, the path of integration in the ω-plane always goes under the Ω pole as illustrated in Fig. 5.2.

5.2 STABILITY CURVE

For a Gaussian distribution, the integral in the dispersion relation is related to the complex error function, so that an analytic solution can be written down. For other distributions, one has to resort to numerical method. For a given growth rate or $\mathcal{I}m\,\Omega$, we perform the integral for various values of $\mathcal{R}e\,\Omega$ and read off $\mathcal{R}e\,Z_0^{\parallel}$ and $\mathcal{I}m\,Z_0^{\parallel}$ from the dispersion equation. Thus, we can plot a contour in the $\mathcal{R}e\,Z_0^{\parallel}$-$\mathcal{I}m\,Z_0^{\parallel}$ plane corresponding to a certain growth rate. This plot for the Gaussian distribution below transition is shown in Fig. 5.3. What are plotted is the real part U' and imaginary part V' of

$$U' + iV' = \frac{eI_0\beta^2(Z_0^{\parallel}/n)}{|\eta|E_0(\Delta E/E)^2_{\rm FWHM}} \tag{5.18}$$

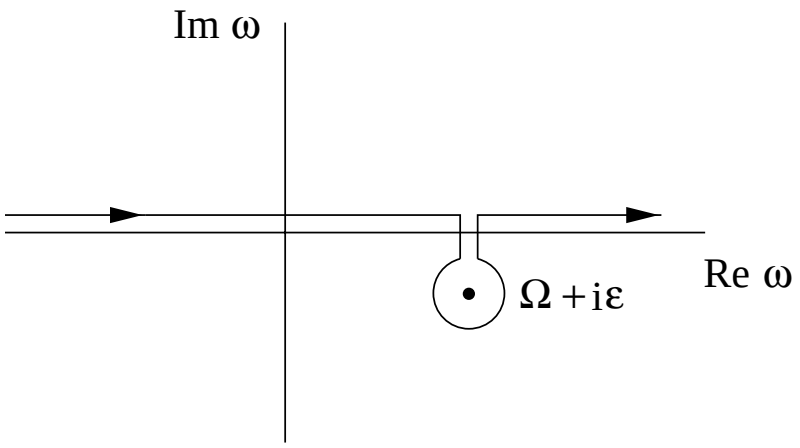

Figure 5.2: The path of integration in the dispersion relation must go below the Ω pole.

at fixed growth rates. From outside to inside, the contours in the figure correspond to growth rates 0.5 to -0.5 in steps of -0.1 in units of HWHM of the frequency spread, where negative values imply damping. The contour corresponding to the stability threshold is drawn in dot-dashes and the area inside it is stable. Note that the positive V'-axis is a cut and those damping contours continue into other Riemann sheets after passing through the cut. Therefore, for each (U', V') outside the stability region bounded by the dot-dashed curve, there can also be one or more stable solutions. However, since there is at least one unstable solution, this outside region is termed unstable.

Obviously, these contours depend on the distribution $g_0(\omega)$ assumed. In Fig. 5.4, we plot the stability contours for various frequency distributions below transition. They are for frequency distributions, from inside to outside, $f(x) = \frac{3}{4}(1-x^2)$, $\frac{8}{3\pi}(1-x^2)^{3/2}$, $\frac{15}{16}(1-x^2)^2$, $\frac{315}{32}(1-x^2)^4$, and $\frac{1}{\sqrt{2\pi}}e^{-x^2/2}$. The innermost one is the parabolic distribution with discontinuous density slopes at the edges and we see that the stability contour curves towards the origin in the positive V' region. The contour next to it corresponds to continuous density slopes at the edges and it does not dip downward in the positive V' region. As the edges become smoother or with higher derivatives that are continuous, the contour shoots up higher in the upper half plane. For all distributions with a finite spread, the contours end with finite values at the positive V'-axis. For the Gaussian distribution which has infinite spread and continuous derivatives up to infinite orders, the contour will only approach the positive V'-axis without intersecting it.

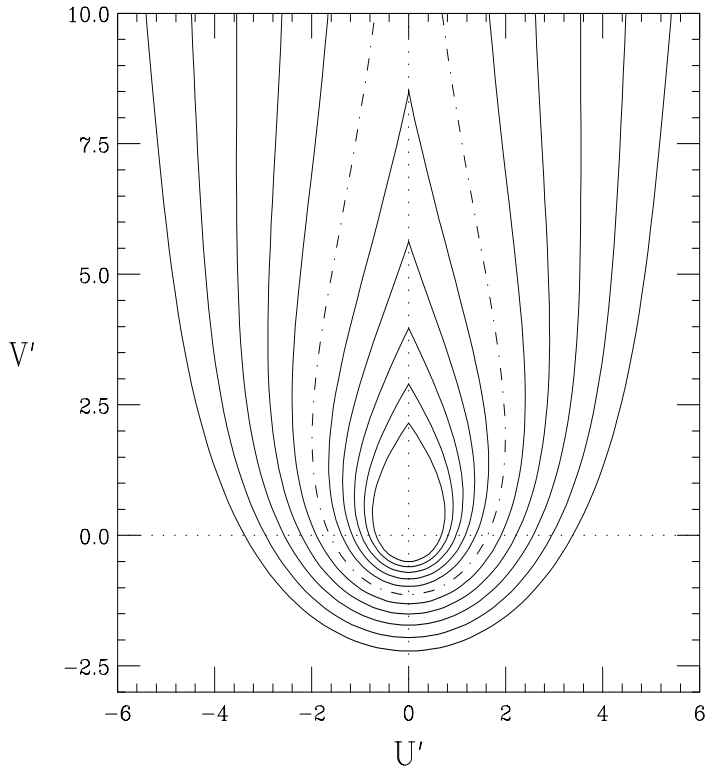

Figure 5.3: The growth contours for a Gaussian distribution in revolution frequency below transition. The abscissa U' and ordinate V' are, respectively, real and imaginary parts of $eI_0\beta^2(Z_0^{\parallel}/n)/[|\eta|E_0(\Delta E/E)^2_{\rm FWHM}]$. From outside to inside, the contours correspond to growth rates 0.5 to -0.5 in steps of -0.1 in units of HWHM of the frequency spread, where negative values imply damping. The contour corresponding to the stability threshold is drawn in dot-dashes and the area inside it is stable.

We note in Fig. 5.4 that, regardless the form of distribution, all contours cut the negative V'-axis at ~ -1. Therefore, it is reasonable to approximate the stability region by a unit circle in the U'-V' plane, so that a stability criterion can be written analytically. This is the *Keil-Schnell criterion* which reads [3]

$$\left|\frac{Z_0^{\parallel}}{n}\right| < F\frac{|\eta|E_0}{eI_0\beta^2}\left(\frac{\Delta E}{E_0}\right)^2_{\rm FWHM}\ , \tag{5.19}$$

where F is a distribution-dependent form factor and is equal to the negative V'-intersection of the contour. For all the distributions discussed here, $F \approx 1$. (See Exercise 5.1 below).

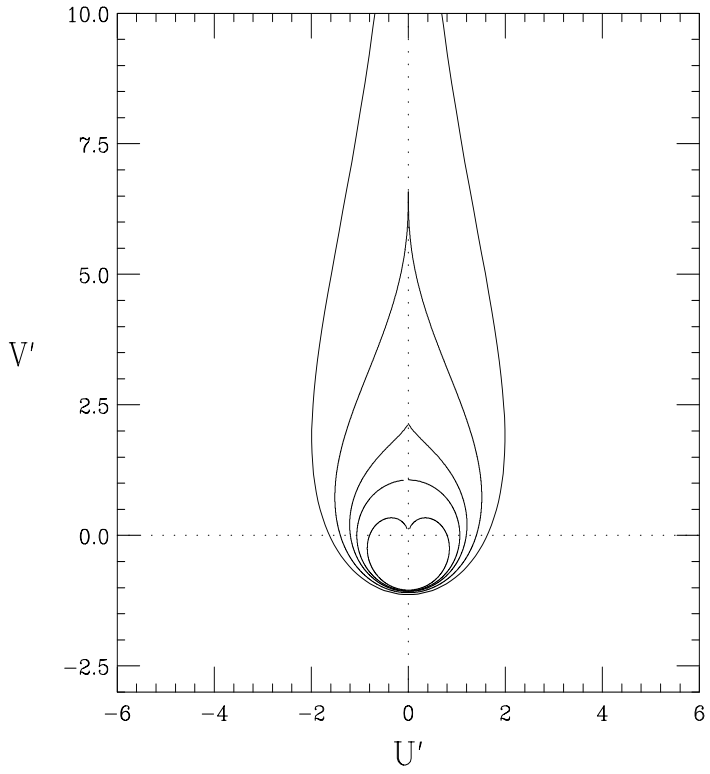

Figure 5.4: The stability contours for different frequency distribution below transition. The abscissa U' and ordinate V' are, respectively, real and imaginary parts of $eI_0\beta^2(Z_0^{\parallel}/n)/[|\eta|E_0(\Delta E/E)^2_{\rm FWHM}]$. From inside to outside, they correspond to unperturbed revolution frequency distribution $f(x) = \frac{3}{4}(1-x^2)$, $\frac{8}{3\pi}(1-x^2)^{3/2}$, $\frac{15}{16}(1-x^2)^2$, $\frac{315}{32}(1-x^2)^4$, and $\frac{1}{\sqrt{2\pi}}e^{-x^2/2}$. Note that all contours cut the V'-axis at about -1.

For a bunch beam, if the disturbance has a wavelength much less than the bunch length, we can view the bunch locally as a coasting beam. Boussard [4] suggested to apply the same Keil-Schnell stability criterion to a bunch beam by replacing the coasting beam current I_0 with the peak current $I_{\rm peak}$ of the bunch. Krinsky and Wang [5] performed a vigorous derivation of the microwave stability limit for a bunch beam with a Gaussian energy spread and found the stability criterion

$$\left|\frac{Z_0^{\parallel}}{n}\right| < \frac{2\pi|\eta|E_0}{eI_{\rm peak}\beta^2}\left(\frac{\Delta E}{E_0}\right)^2_{\rm rms} \quad . \tag{5.20}$$

Comparing with Eq. (5.19), the Krinsky-Wang criterion corresponds to the Keil-Schnell criterion with a form factor of $\pi/(4\ln 2) = 1.133$, which is exactly the negative V'-intersect (see Exercise 5.1.)

5.3 LANDAU DAMPING

Keil-Schnell Criterion can be written as

$$n\omega_0\sqrt{\frac{e|\eta||Z_0^{\parallel}/n|I_0}{2\pi\beta^2E_0}} < n\omega_0\sqrt{\frac{F}{2\pi}}\frac{|\eta|\Delta E|_{\rm FWHM}}{\beta^2E_0} \ . \tag{5.21}$$

The left side is the growth rate as discussed in Eq. (5.14) with I_0 replaced by $I_{\rm peak}$ in the case of a bunch. The right side can therefore be considered as the Landau damping rate coming from energy spread or frequency spread. Stability is maintained if Landau damping is large enough. The theory of Landau damping is rather profound, for example, the exchange of energy between particles and waves, the mechanism of damping, the contour around the poles in Eq. (5.12), etc. The readers are referred to the papers by Landau and Jackson [1, 6], and also a very well-written chapter in Chao's book [2].

5.4 SELF-BUNCHING

Neglecting the effect of wake function, the Hamiltonian for particle motion can be written as

$$H = -\frac{\eta}{2v\beta^2E_0}(\Delta E)^2 + \frac{eV_{\rm rf}}{2\pi vh}\cos(h\omega_0\tau) \ , \tag{5.22}$$

where the synchronous angle has been put to zero and the small-bunch approximation has been relaxed. It is easy to see that the height of the bucket is

$$\Delta E|_{\rm bucket} = \sqrt{\frac{eE_0V_{\rm rf}}{\pi h|\eta|}} \ . \tag{5.23}$$

Keil-Schnell criterion can also be written as

$$\sqrt{\frac{eE_0I_0|Z_0^{\parallel}|}{\pi n|\eta|}} < \sqrt{\frac{F}{\pi\beta^2}}\Delta E|_{\rm FWHM} \ . \tag{5.24}$$

Comparing with Eq. (5.23), the left side can be viewed as the height of a bucket created by an induced voltage $I_0|Z_0^{\parallel}|$ while the right side roughly the half full energy spread of the beam. This induced voltage will bunch the beam just as an rf voltage does. If the self-bunched bucket height is less than the half full energy spread of the beam, the bunching effect will not be visible and beam remains coasting. Otherwise, the beam breaks

up into bunchlets of harmonic n, and we call it unstable. This mechanism is known as *self-bunching*.

5.5 OVERSHOOT

When the current is above the microwave threshold, the self-bunching concept tells us that there will be an increase in energy spread of the beam. The increase continues until it is large enough to stabilize the beam again according to the Keil-Schnell criterion. For a proton beam, experimental observation indicates that there will be an overshoot. Let $(\Delta E)_i$ be the initial energy spread which is below the threshold energy spread $(\Delta E)_{\rm th}$ postulated by the Keil-Schnell criterion. The final energy spread $(\Delta E)_f$ was found to be given empirically by [7]

$$(\Delta E)_i(\Delta E)_f = (\Delta E)^2_{\rm th} \ . \tag{5.25}$$

Thus the final energy spread is always larger than the threshold energy spread. An overshoot formula similar to but not exactly the same as Eq. (5.25) has been derived by Chin and Yokoya [8], and Bogacz and Ng [9]. For a bunch, the rf voltage introduces synchrotron oscillations. Thus, an increase in energy spread implies also eventual increase in bunch length. At the same time, the bunch area will be increased also.

The situation is quite different for electron bunches because of radiation damping. This will be discussed in Chapter 6.

5.6 OBSERVATION AND CURE

In order for a bunch to be microwave unstable, the growth rate has to be much faster than the synchrotron frequency. For the Fermilab Main Ring, the synchrotron period was typically about 100 to 200 turns or 2 to 4 ms. A naive way is to observe the microwave growth is to view the spectrum of the bunch over a large range of frequencies at a certain moment. However, the bunch spectrum produced by a network analyzer is usually via a series of frequency filters of narrow width, starting from low frequencies and working its way towards high frequencies. This process is time consuming. As soon as the filtering reaches the frequencies concerned, typically a few GHz, the microwave growth may have been stabilized already through bunch dilution, and therefore no growth signals will be recorded. The correct way is to set the network analyzer at a narrow frequency span

and look at the beam signal as a function of time. The frequency span is next set to an adjacent frequency interval and the observation repeated until the frequency range of a few GHz has been covered. Besides, we must make sure that the network analyzer is capable of covering the high frequency of a few GHz for the microwave growth signals. Also the cable from the beam detector to the network analyzer must be thick enough so that high-frequency attenuation is not a problem in signal propagation.

Since microwave instability occurs so fast, it is not possible to use a damper system to cure it. One way to prevent the instability is to blow up the bunch so that the energy spread is large enough to provide the amount of Landau damping needed. Another way is to reduce the impedance budget of the ring by smoothing out the beam pipe discontinuities. For negative-mass instability driven by the space-charge impedance just after transition, one can try to modify the ramp curve so that transition can be crossed faster. Of course, a γ_t-jump mechanism will be very helpful.

5.7 FERRITE INSERTION AND INSTABILITY

In Sec. 4.5, we discuss an experiment at the Los Alamos PSR where the space-charge repulsive force is large compared with the available rf bunching force. Ferrite rings were installed into the vacuum chamber so that the beam would see an amount of inductive force from the ferrite. The experiment results show that this additional inductive force did cancel an appreciable amount of the space-charge force of the intense proton beam. This is evident because the bunch lengths were shortened in the presence of the ferrite with zero bias of the solenoidal current wound outside the ferrite tuners, and lengthened when the ferrite rings were biased. Also, the rf voltage required to keep the protons bunched to the required length had been lowered by about 1/3 in the presence of the ferrite insertion. However, the space-charge compensation of the potential-well distortion has not been perfect. The ferrite insertion did lead to serious instability which we are going to discuss below.

5.7.1 MICROWAVE INSTABILITY

The PSR was upgraded in 1998. After that all three ferrite tuners were installed in order to cope with the higher intensity beam. However, instability was observed.

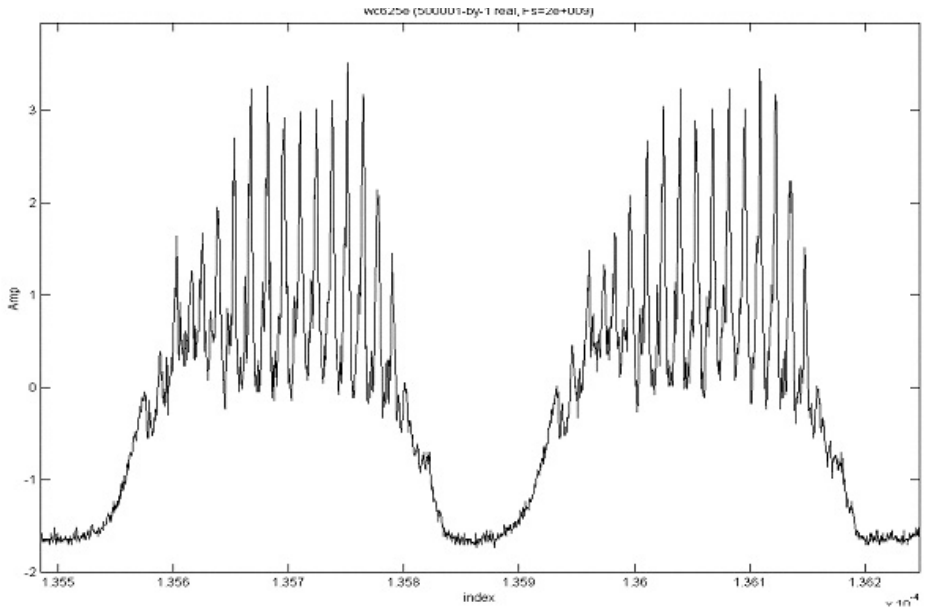

Figure 5.5: Beam profile of two consecutive turns of a chopped coasting beam recorded in a wall-gap monitor after storage of ~ 500 μs. The ripples show a longitudinal microwave instability has occurred.

Figure 5.5 shows two consecutive turns of a chopped coasting beam (with the rf buncher off) accumulated for 125 μs and stored for 500 μs recorded at a wide-band wall current monitor. The ripples at the beam profile indicate a longitudinal microwave instability has occurred. The FFT spectrum in Fig. 5.6 shows that the instability is driven at 72.7 MHz or the 26th revolution harmonic. Ripples also show up at the rear half of a bunch, as recorded by a wall-gap monitor in Fig. 5.7. The top plots are two successive turns of a ~ 250 ns (full width) bunch. Apparently, the instability is tolerable because ripples do not distort the shape of the bunch by too much. However, the ~ 100 ns bunch on the bottom plots is totally disastrous. The instability lengthens the bunch to almost 200 ns with very noticeable head-tail asymmetry.

5.7.2 CAUSE OF INSTABILITY

In order to understand the reason of the instability, let us first build a simple model for the ferrite tuner. To incorporate loss, the relative permeability of the ferrite can be

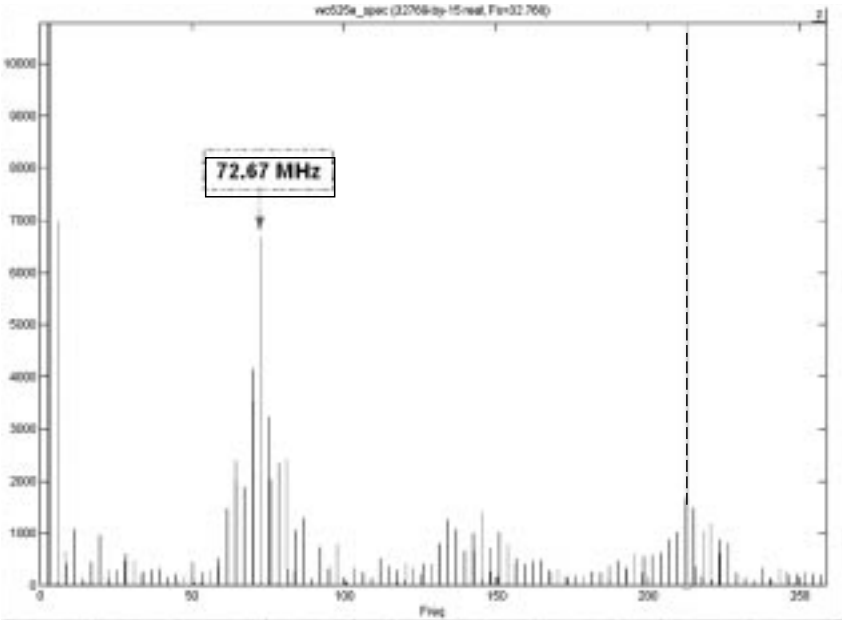

Figure 5.6: Spectrum of the instability signal of the chopped beam in Fig. 5.5, showing the driving frequency is at 72.7 MHz.

made complex: $\mu \to \mu' + i\mu''$. The impedance of the ferrite is therefore

$$\frac{Z_0^{\parallel}}{n} = -i(\mu' + i\mu'')\omega_0 L \ , \tag{5.26}$$

where L denotes the inductance of the ferrite required to compensate for the space charge of the bunch. It is clear that μ' and μ'' must be frequency-dependent. Their general behaviors are shown in Fig. 5.8. For the Toshiba M_4C_{21A} ferrite, μ' is roughly constant at $\mu'_L \sim 70$ at low frequencies and starts to roll off around $\omega_r/(2\pi) \sim 50$ MHz, while μ'', being nearly zero at low frequencies, reaches a maximum μ''_R near $\omega_r/(2\pi)$. The simplest model for a piece of ferrite consists of an *ideal* inductance L and an *ideal* resistor R in parallel, which gives

$$Z(\omega) = -i\omega L \frac{1 + i\omega/\omega_r}{1 + \omega^2/\omega_r^2} \propto -i\omega(\mu'_s + i\mu''_s) \ , \tag{5.27}$$

with a resonance at

$$\omega_r = \frac{R}{L} \ . \tag{5.28}$$

We see that the series μ'_s is relatively constant at low frequencies and rolls off near ω_r, while μ''_s increases as ω at low frequencies and resonates at ω_r. The corresponding longitudinal

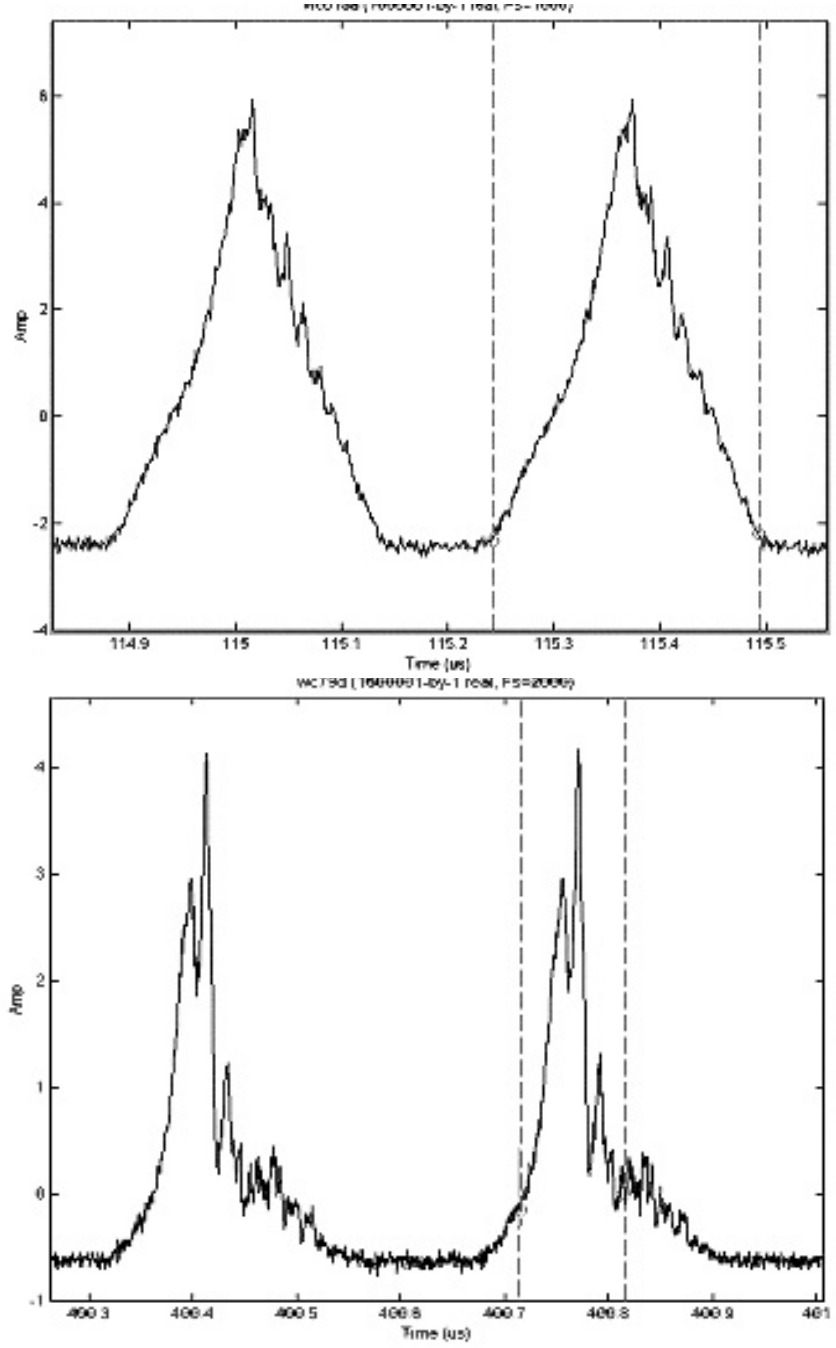

Figure 5.7: Instability perturbation on profiles of bunches with full width 250 ns (top) and 100 ns (bottom). The effect on the 250 ns bunch may be tolerable, but certainly not on the 100 ns bunch, which has lengthened almost to 200 ns.

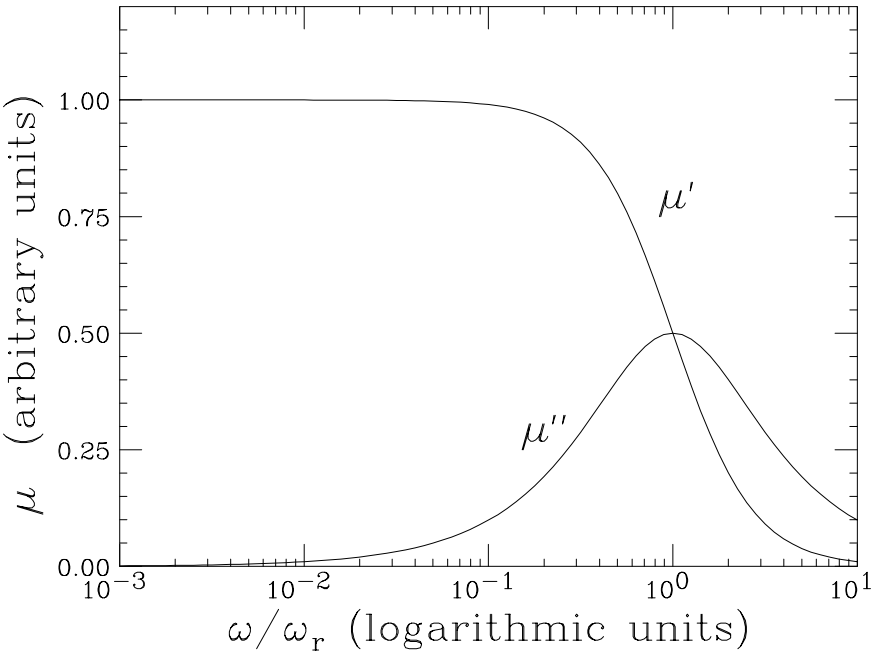

Figure 5.8: (color) Plot of μ' and μ'' as functions of frequency in the 2-parameter model. These are the typical properties of μ' and mu'' for most ferrites.

wake potential is

$$W(\tau) = R\,[\,\delta(\tau) - \omega_r e^{-\omega_r \tau}\,]\,. \tag{5.29}$$

When the ferrite is biased, L decreases so that μ' decreases. In this model, this is accomplished by raising the resonant frequency ω_r. Actually, measurements show that the resonant frequency of μ'' does increase when the ferrite is biased. Thus, this simple 2-parameter model gives a very reasonable description of the ferrite.

With the ferrite rings enclosed in a pill-box cavity, a 3-parameter broadband parallel-RLC resonance model appears to be more appropriate. We have

$$Z_0^{\parallel}(\omega) = \frac{R}{1 - iQ\left(\dfrac{\omega}{\omega_r} - \dfrac{\omega_r}{\omega}\right)}\,, \tag{5.30}$$

where ω_r is roughly where μ'' peaks. The other two parameters R and Q can be obtained in terms of μ'_L, the value of μ' at low frequencies, and μ''_R, the value of μ'' at resonant

frequency $\omega_r/(2\pi)$. From Eq. (5.26), we obtain

$$\left|\frac{Z_0^{\parallel}}{n}\right|_{\rm ind} = \mu'_L \omega_0 L \qquad \text{and} \qquad \mathcal{R}e\, Z_0^{\parallel}(\omega_r) = \mu''_R \omega_r L \ , \tag{5.31}$$

where $|Z_0^{\parallel}/n|_{\rm ind}$ is the inductor impedance per harmonic. From Eq (5.30), we obtain

$$\left|\frac{Z_0^{\parallel}}{n}\right|_{\rm ind} = \frac{\omega_0 R}{Q\omega_r} \qquad \text{and} \qquad \mathcal{R}e\, Z_0^{\parallel}(\omega_r) = R \ . \tag{5.32}$$

Thus, we can solve for $\mu''_R = Q\mu'_L$. Note that Q here is the quality factor describing the μ'' peak. It relates the values of μ' and μ'' at *different* frequencies, and is not the usual industrial-quoted Q which relates them at the *same* frequency.

For a space-charge dominated beam, the actual area of beam stability in the complex $Z_0^{\parallel}$-plane (or the traditional U'-V' plane) is somewhat different from the commonly quoted Keil-Schnell estimation. In Fig. 5.9, the heart-shape solid curve, denoted by 1, is the threshold curve for parabolic distribution in momentum spread, where the momentum gradient is discontinuous at the ends of the spread. Instability develops and a smooth momentum gradient will result at the ends of the spread, changing the threshold curve to that of a distribution represented by 2, for example, $\frac{15}{16}(1-\delta^2/\hat{\delta}^2)^2$. Further smoothing of the momentum gradient at the ends of the spread to a Gaussian distribution will change the threshold curve to 3. On the other hand, the commonly known Keil-Schnell threshold is denoted by the circle of unit radius in dots. This is the reason why in many low-energy machines the Keil-Schnell limit has been significantly overcome by a factor of about 5 to 10. In this case, the space charge is almost the only source of the impedance, the real part of the impedance can be typically orders of magnitude smaller. As an example, if the impedance of the Los Alamos PSR is at Point A, the beam is within the microwave stable region if the momentum spread is Gaussian like, although it exceeds the Keil-Schnell limit. Now, if we compensate the space-charge potential-well distortion by the ferrite inductance, the ferrite required will have an inductive impedance at low frequency equal to the negative value of the space charge impedance at A, for example, about -5.5 units according to Fig. 5.9. However, the ferrite also has a resistive impedance or $\mathcal{R}e\, Z_0^{\parallel}$. Although $\mathcal{R}e\, Z_0^{\parallel}/n$ is negligible at low frequencies (for example, the rf frequency of 2.796 MHz of the PSR), it reaches a peak value near $\omega_r/(2\pi)$ (about 50 to 80 MHz for the Toshiba M_4C_{21A} inside the pill-box container) with the peak value the same order of magnitude as the low-frequency $\mathcal{I}m\, Z_0^{\parallel}$. Actually, according to the RLC model discussed

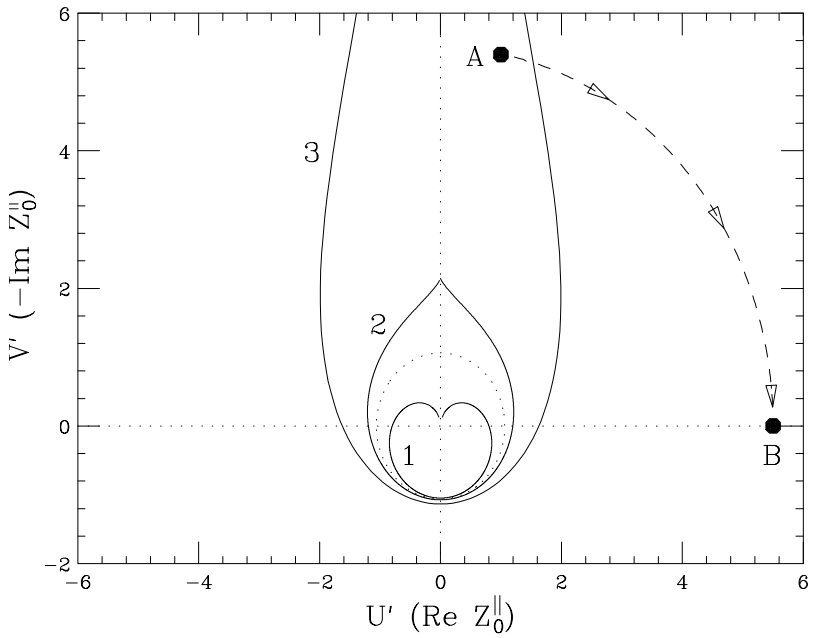

Figure 5.9: Microwave instability threshold curves in the complex $Z_0^{\|}$ (or U'-V') plane, for (1) parabolic momentum distribution, (2) distribution with a continuous momentum gradient, and (3) Gaussian momentum distribution. The commonly quoted Keil-Schnell threshold criterion is denoted by the circle in dots. An intense space-charge beam may have impedance at Point A outside the Keil-Schnell circle and is stable. A ferrite tuner compensating the space charge completely will have a resistive impedance roughly at Point B and is therefore unstable.

above, we get

$$\frac{\mathcal{R}e\, Z_0^{\|}/n|_{\rm pk}}{\mathcal{I}m\, Z_0^{\|}/n|_{\omega\to 0}} \approx \frac{Q^2+Q+1}{Q+2} = \left\{ \begin{array}{ll} Q & \text{if } Q \gg 1 \\ 1 & \text{if } Q \sim 1 \\ \frac{1}{2} & \text{if } Q \ll 1 \end{array} \right\} \geq \frac{1}{2}\,. \tag{5.33}$$

The RL model gives the same impedance ratio of $\frac{1}{2}$ as the low-Q case of Eq.(5.33). Thus the ferrite will contribute a resistive impedance denoted roughly by Point B (~ 5.5 units) when $Q \sim 1$ or at least one half of it when $Q \ll 1$. This resistive impedance of the ferrite will certainly exceed the threshold curve and we believe that the longitudinal instability observed at the Los Alamos PSR is a result of this consideration. It follows from here that such low-frequency compensation of an intense space-charge induced potential-well distortion will result in the microwave instability at high frequencies, $\omega \simeq \omega_r$. In other

words, the strong space-charge potential-well distortion can only be compensated by the ferrite inductance to a small extent to ensure that the resistive part of the ferrite is kept below the microwave instability threshold.

5.7.3 HEATING THE FERRITE

One way to avoid the longitudinal microwave instability driven by the compensating ferrite is to choose a ferrite having the properties of high μ' at low frequencies and low μ'' at the resonant frequency. Their ratio should be at least larger than 10. It was pointed out by Popovic [10] that when a piece of ferrite is heated up, μ' will increase and the μ'' will decrease, thus having exactly the same properties that we are looking for. A wire was wrapped through a Toshiba ferrite ring and a voltage was applied at a particular frequency. The voltage, current, and the phase between them were recorded. The real and imaginary parts of the relative magnetic permeability were inferred with the aid of Eq. (4.47). The results of the measurement from 10 to 100 MHz at room temperature 23°C, 100°C, and 150°C are plotted in Fig. 5.10. The situation at 23°C is at the bottom left. It is plotted again at the top left at the same scale as the measurements made at 100°C (top right) and 150°C (bottom right). It is important to point out that this method of measurement may not be accurate, especially at higher frequencies. This is because at high frequencies, the contribution of the capacitance of the wire loop cannot be neglected and it contaminates the measurement data. That explains why unphysical numbers are shown in Fig. 5.10; namely μ' becomes negative at high frequencies, and also the peak values of μ'' are larger than the low-frequency values of μ'. Nevertheless, the results do give a relative measurement of the relative permeability between different temperature.

We see that when the temperature is raised from 23°C to 150°C, the "μ''" resonant peak drops roughly 6 fold from ~ 6000 to ~ 100. At the same time μ' increases by 29% from 328 to 422. Another measurement has been made by sending a sinusoidal wave from one end of the ferrite tuner via an antenna and receiving the wave with an antenna at the other end. The measurement also reveals that the μ'' resonant peak drops by a factor of about 6.

At Los Alamos, the solenoidal wires of the ferrite tuners were removed and the outside of the tuners were wound with heating tapes. Two of the tuners were reinstalled into the PSR ring. By heating the ferrite tuners up to 130°C, the longitudinal microwave instability disappears. The profile of the 100 ns bunch in the presence of the heated ferrite tuners

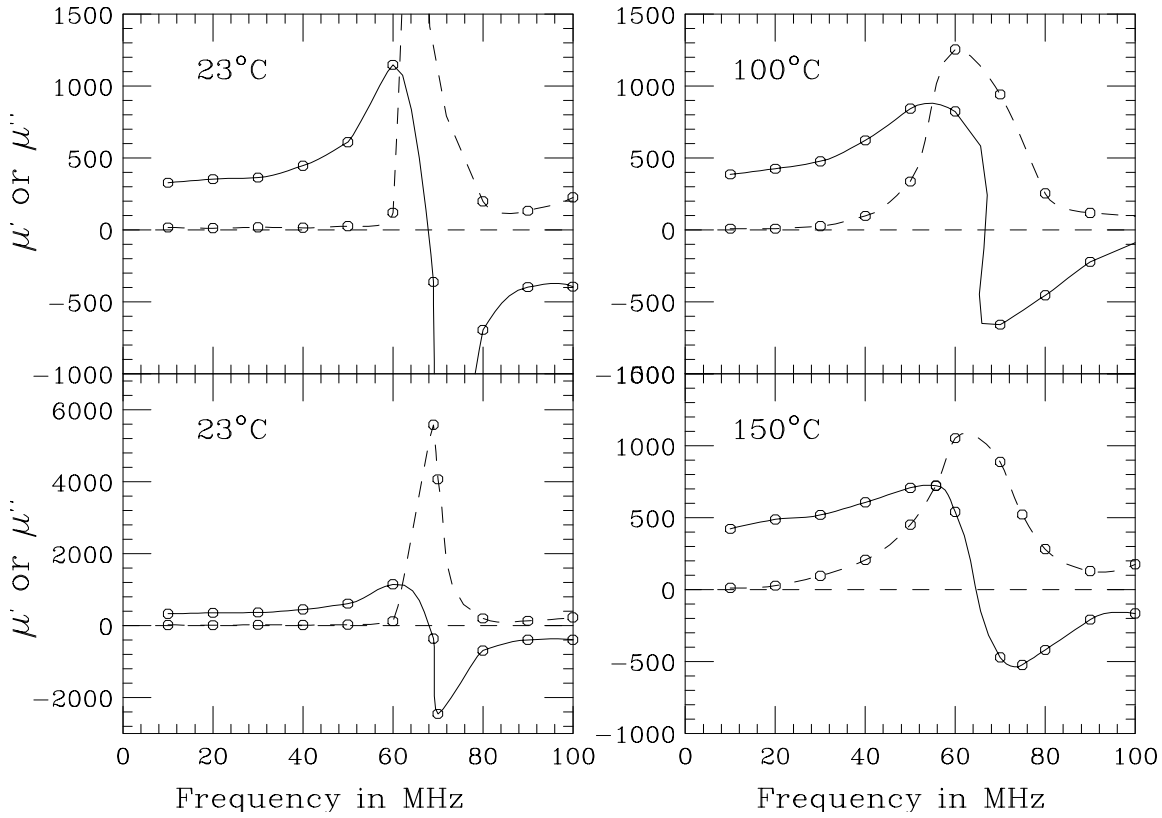

Figure 5.10: Measurement results of μ' and μ'' up to 100 MHz at 23°C, 100°C, and 150°C. The top left and bottom left are both at 23°C but at different vertical scales. Note that the measurement is not accurate at all at high frequencies because of the capacitance of the wire loop becomes no longer negligible. Thus, the data should be treated as relative between different temperatures.

is shown in Fig. 5.11. Comparing with the bottom plot of Fig. 5.7, it is evident that the bunch profile is in good shape, the bunch has not been lengthened, and there is no more sign of microwave instability. At the present, the PSR with two heated ferrite tuners can run at an intensity over 5×10^{13} with all the space charge compensated but without any sign of longitudinal microwave instability.

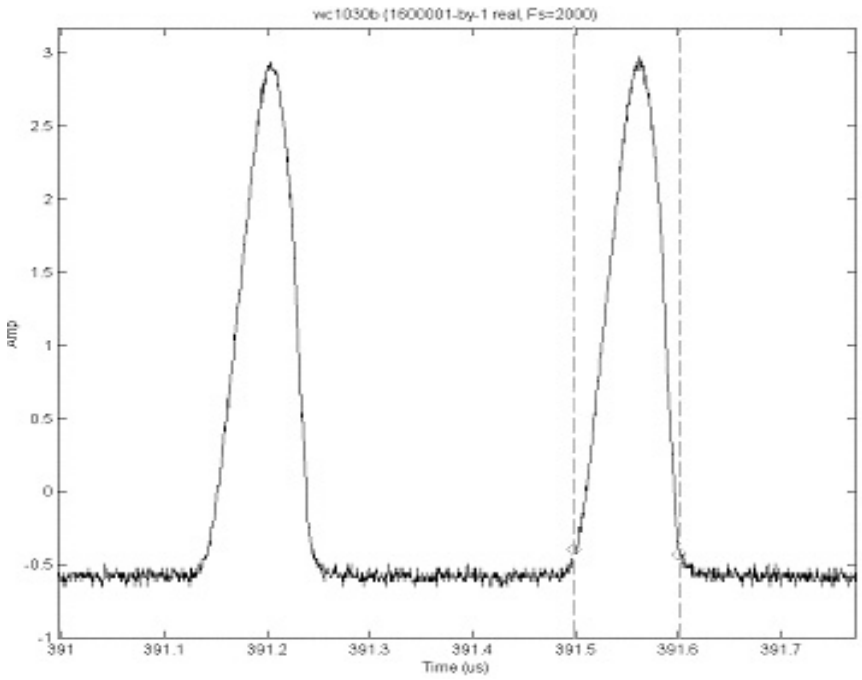

Figure 5.11: With two ferrite tuners installed and heated to 130°C, the instability ripples disappear from the profile of the 100 ns bunch.

5.8 EXERCISES

5.1. The dispersion relation of Eq. (5.16) can be rewritten in a simpler form. let us measure revolution angular frequency in terms of $2S$, the FWHM spread, which is related to the FWHM energy spread by

$$2S = -\eta\omega_0 \left.\frac{\Delta E}{E_0}\right|_{\text{FWHM}} . \tag{5.34}$$

We can then introduce a dimensionless reduced angular frequency x such that

$$n\omega - n\omega_0 = nxS \qquad \text{and} \qquad \Omega - n\omega_0 = nx_1S \ , \tag{5.35}$$

where we have used the fact the the collective angular frequency Ω in Eq. (5.14) is close to $n\omega_0$. The frequency distribution function $g_0(\omega)$ is now transformed to a distribution $f(x)$ which is normalized to 1 when integrated over x. We have

$$\frac{dg_0(\omega)}{d\omega}d\omega = \frac{d\,f(x)}{dx}\frac{dx}{d\omega}dx = \frac{1}{S}\frac{d\,f(x)}{dx}dx \ . \tag{5.36}$$

(a) Show that the dispersion relation (5.16) becomes

$$1 = -\frac{i2\,\mathrm{sgn}(\eta)}{\pi}(U' + iV')\int \frac{f'(x)}{x_1 - x}dx \ , \tag{5.37}$$

where U' and V' are defined in Eq. (5.18).

(b) When the beam current is just above threshold, the reduced collective angular frequency is written as $x_1 = x_{1R} + i\epsilon$ where x_{1R} is real and ϵ is an infinitesimal positive number. Show that the stability curve can be obtained from

$$1 = -\frac{i2\,\mathrm{sgn}(\eta)}{\pi}(U' + iV')\left[\wp\int \frac{f'(x)}{x_{1R} - x}dx - i\pi f'(x_{1R})\right] \ . \tag{5.38}$$

by varying x_{1R}, where $\wp$ denotes the principal value of the integral.

(c) show that the negative V'-intersect or the lowest point of the bell-shaped stability curve V'_{in} is given by

$$1 = -\frac{2\,\mathrm{sgn}(\eta)V'_{\mathrm{in}}}{\pi}\,\wp\int \frac{f'(x)}{x}dx \ . \tag{5.39}$$

In fact, the form factor in the Keil-Schnell criterion is given by $F = |V'_{\mathrm{in}}|$.

(d) The form factor F's in the Keil Schnell criterion for various frequency distribution functions are listed in Table 5.1. Verify the results.

5.2. Using Eq. (5.38), plot the bell-shaped stability contours for the distributions listed in Table 5.1 as illustrated in Fig. 5.4.

5.3. Using Eq. (5.37), show that the constant-growth contours for the Gaussian distribution are given by

$$1 = \frac{i\,\mathrm{sgn}(\eta)4\ln 2}{\pi}(U' + iV')\left[1 + i\sqrt{\pi\ln 2}\ x_1\, w(\sqrt{\ln 2}\, x_1)\right] \ , \tag{5.40}$$

where use has been made of the integral representation of the complex error function:

$$w(z) = \frac{i}{\pi}\int_{-\infty}^{\infty}\frac{e^{-t^2}}{z - t}dt \qquad \text{for } \mathcal{I}m\, z > 0 \ . \tag{5.41}$$

Plot the contours in Fig. 5.3.

Table 5.1: Form factors in the Keil-Schnell criterion for various distributions. For the first four, the distributions reside only inside the region $|\Delta\omega| \leq \widehat{\Delta\omega}$. When normalized to the HWHM, the domain becomes $|x| \leq a$.

Frequency Distribution			**Form Factor**
$g_0(\omega) \qquad [\Delta\omega = \omega - \omega_0]$	$f(x)$		F
$\dfrac{3}{4\widehat{\Delta\omega}}\left(1-\dfrac{\Delta\omega^2}{\widehat{\Delta\omega}^2}\right)$	$\dfrac{3}{4a}\left(1-\dfrac{x^2}{a^2}\right)$	$a^2 = 2$	$\dfrac{\pi a^2}{6} = 1.0472$
$\dfrac{8}{3\pi\widehat{\Delta\omega}}\left(1-\dfrac{\Delta\omega^2}{\widehat{\Delta\omega}^2}\right)^{3/2}$	$\dfrac{8}{3\pi a}\left(1-\dfrac{x^2}{a^2}\right)^{3/2}$	$a^2 = \dfrac{1}{1-2^{-2/3}}$	$\dfrac{\pi a^2}{8} = 1.0612$
$\dfrac{15}{16\widehat{\Delta\omega}}\left(1-\dfrac{\Delta\omega^2}{\widehat{\Delta\omega}^2}\right)^{2}$	$\dfrac{15}{16a}\left(1-\dfrac{x^2}{a^2}\right)^{2}$	$a^2 = \dfrac{1}{1-2^{-1/2}}$	$\dfrac{\pi a^2}{10} = 1.0726$
$\dfrac{315}{256\widehat{\Delta\omega}}\left(1-\dfrac{\Delta\omega^2}{\widehat{\Delta\omega}^2}\right)^{4}$	$\dfrac{315}{256a}\left(1-\dfrac{x^2}{a^2}\right)^{4}$	$a^2 = \dfrac{1}{1-2^{-1/4}}$	$\dfrac{\pi a^2}{18} = 1.0970$
$\dfrac{1}{\sqrt{2\pi}\sigma}\exp\left(-\dfrac{\Delta\omega^2}{2\sigma^2}\right)$	$\dfrac{1}{\sqrt{2\pi}a}\exp\left(-\dfrac{x^2}{2a^2}\right)$	$a^2 = \dfrac{1}{2\ln 2}$	$\dfrac{\pi a^2}{2} = 1.1331$

Bibliography

[1] L.D. Landau, J. Phys. USSR **10**, 25 (1946);

[2] A.W. Chao, *Physics of Collective Beam Instabilities in High Energy Accelerators*, John Wiley & Sons, 1993, p. 251.

[3] E. Keil and W. Schnell, CERN Report TH-RF/69-48 (1969); V.K. Neil and A.M. Sessler, Rev. Sci. Instr. **36**, 429 (1965).

[4] D. Boussard, CERN Report Lab II/RF/Int./75-2 (1975).

[5] S. Krinsky and J.M. Wang, Particle Accelerators **17**, 109 (1985).

[6] J.D. Jackson, Plasma Phys. **C1**, 171 (1960).

[7] R.A. Dory, Thesis, MURA Report 654, 1962.

[8] Y. Chin and K. Yokoya, Phys. Rev. **D28**, 2141 (1983).

[9] S.A. Bogacz and K.Y. Ng, Phys. Rev. **D36**, 1538 (1987).

[10] M. Popovic, private communication.